Available online at www.sciencedirect.com

ScienceDirect

Geochimica et Cosmochimica Acta 239 (2018) 49–60

Geochimica et Cosmochimica Acta

www.elsevier.com/locate/gca

Iron isotope pathways in the boreal landscape: Role of the riparian zone

Johan Ingri [a,*], Sarah Conrad [a], Fredrik Lidman [d], Fredrik Nordblad [a], Emma Engström [a,b], Ilia Rodushkin [b], Don Porcelli [c]

[a] Applied Geochemistry, Luleå University of Technology, 971 87 Luleå, Sweden
[b] ALS Laboratory Group, ALS Scandinavia AB, Aurorum 10, 971 75 Luleå, Sweden
[c] Department of Earth Sciences, University of Oxford, South Parks Road, Oxford OX1 3AN, UK
[d] Department of Forest Ecology and Management, Swedish University of Agricultural Sciences, Umeå, Sweden

Received 20 November 2017; accepted in revised form 23 July 2018; available online 4 August 2018

Abstract

Stable Fe isotope compositions have been measured in water samples of the subarctic Kalix River, a first-order stream, and soil water samples from a riparian soil profile adjacent to the first-order stream (Northern Sweden). In the first-order stream, dominated by forest, both the particulate (>0.22 μm) and dissolved (<0.22 μm) phase showed negative δ^{56}Fe values (relative to IRMM-014) during base flow and meltwater discharge in May (−0.97 to −0.09‰). The Fe isotope composition in the water from the riparian soil profile varied between −0.20 and +0.91‰ with sharp gradients near the groundwater table. A linear correlation between the δ^{56}Fe values and the TOC/Fe_{bulk} ratio was measured during snowmelt in the unfiltered river waters (δ^{56}Fe from −0.02 to +0.54‰), suggesting mixing of two Fe components. Two groups of Fe aggregates, with different Fe isotope compositions, are formed in the boreal landscape. We propose that carbon-rich aggregates, Fe(II)(III)-OC, have negative δ^{56}Fe values and Fe-oxyhydroxides have positive δ^{56}Fe values. A mixture of these two components can explain temporal variations of the Fe isotope composition in the Kalix River. This study suggests that stable Fe isotopes can be used as a tool to track and characterize suspended Fe-organic carbon aggregates during transport from the soil, via first-order streams and rivers, to coastal sediment. Furthermore, the differences in Fe isotope values in the Kalix River and the first-order stream during base flow conditions suggest that the primary Fe sources for river water change throughout the year. This model is combining the Fe isotope composition of first-order streams and rivers to weathering and transport processes in the riparian soil.

Keywords: Fe aggregates; Fe isotope; soilwater; Krycklan Catchment; first-order stream; snowmelt; spring flood

1. INTRODUCTION

Iron species in stream and river waters persist mainly as particles and colloids in the micrometer to sub-micrometer size range. Iron-organic carbon (Fe-OC) aggregates are an important carrier phase for metal transport in the boreal landscape (Hamon et al., 2005; Neubauer et al., 2013). Iron-rich aggregates show strong association with OC, and co-precipitation between Fe and OC plays a crucial role in controlling the structure, reactivity, and mobility of natural Fe colloids and particles. Co-precipitation of Fe and dissolved organic carbon (DOC) is common in organic-Fe-rich systems with significant variations in redox state and/or pH (e.g., Pokrovsky and Schott, 2002). Two main pools of Fe, consisting of Fe(II)(III)-OC complexes and Fe-oxyhydroxides were identified by Sundman et al. (2014). Iron(II) rich phases are prevalent throughout oxic aquatic regimes (von der Heyden et al., 2014). Allard et al. (2004) identified two pools of Fe using ultrafiltration

* Corresponding author.
E-mail address: Johan.Ingri@ltu.se (J. Ingri).

https://doi.org/10.1016/j.gca.2018.07.030
0016-7037/

and paramagnetic resonance spectroscopy. The origin and pathways of these two Fe species are unclear. We propose that the two types of Fe aggregates present in stream and river waters can be traced using Fe isotopes. The most significant changes in the Fe isotope composition occurs between the oxidized and reduced phases of Fe, where Fe(III) species tend to have higher $^{56}Fe/^{54}Fe$ isotope values (Polyakov and Mineev, 2000; Anbar et al., 2005). The Fe isotope composition varies in organic-rich rivers with high Fe concentrations. Bergquist and Boyle (2006) showed that the Negro River, Brazil, has positive $\delta^{56}Fe$ values in the dissolved fraction and negative $\delta^{56}Fe$ values in the particulate fraction. Similarly, several studies have shown two groups of Fe isotope compositions in rivers (Escoube et al., 2009, 2015; Ilina et al., 2013; Mulholland et al., 2015). The processes behind the formation of these two groups and temporal variations are unclear. Patel-Sorrentino et al. (2007) concluded that soils actively control the physicochemical characteristics in stream water. Solid soils display a range of variations in the $\delta^{56}Fe$ values from −0.61‰ to +1.04‰ (e.g. Emmanuel et al., 2005; Wiederhold et al., 2007a,b; Poitrasson et al., 2008; Huang et al., 2018), indicating that pedogenic processes generate Fe isotope fractionation. Dos Santos Pinheiro et al. (2014) suggested that variations in the Fe isotope composition in the Negro River suspended matter indicate that a negative $\delta^{56}Fe$ composition (fractionated during pedogenesis) is transported from soils to the river, especially during storm events. The changing redox state at the stream water-soil interface influences the Fe isotope composition. It is essential to study Fe isotopes in defined small catchments (first-order streams) to understand the Fe isotope composition in rivers and estuaries. We have analyzed Fe isotopes in three key compartments in the boreal landscape: a major river (Kalix River), riparian soil water, and a first-order stream, dominated by forest.

2. STUDY AREA

Several studies investigated the geochemistry of the Kalix River (e.g., Ingri and Widerlund, 1994; Ingri et al., 2000, 2005, 2006; Andersson et al., 2006; Dahlqvist et al., 2007; Engström et al., 2010). The river is pristine and has no dams. Samples were taken close to the river mouth, at Kamlunge (Fig. 1). Kalix River has its source in the Caledonian Mountains, dominated by mica schist, quartzite, and amphibolite, and flows into the Bothnian Bay. Granite dominates in the rest of the catchment (Gaál and Gorbatschev, 1987). The drainage area consists of forest (55–65%), peatland (17–20%), lakes (4%) and farmland cover (<1%) (after SMHI, 2018). Till covers the granitic bedrock below the mountains. In the forested lowland the till shows well-developed podzol profiles (Fromm, 1965). Podzol profiles typically consist of, from top to bottom, (1) the O-horizon, which is a black or dark brown organic-rich layer, (2) the E-horizon, which is a gray sandy and silty layer, as minerals, organic matter, and clays are leached out of the layer, (3) the B-horizon, enriched by illuviation and coloured by organic matter (Bh) and iron oxides (Bs) (Wiederhold et al., 2007a), (4) the C-horizon, containing relatively unweathered rock fragments and lacks

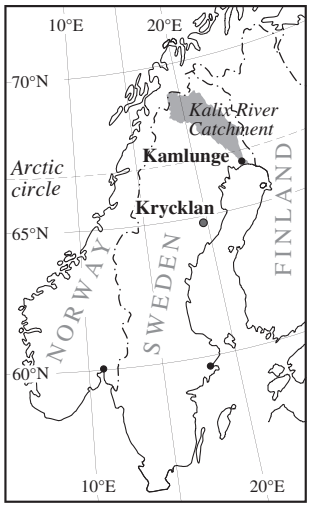

Fig. 1. The Kalix River catchment is displayed in light gray, showing the sampling station of Kamlunge close to the river mouth. The Krycklan Catchment is shown as a single dot, including the sampling station Västrabäcken.

organic materials. The process of developing a podzol profile is called podzolization (e.g. Anderson et al., 1982; Lundström et al., 2000; Buurman and Jongmans, 2005; Sauer et al., 2007, 2008; Cornu et al., 2009; Fekiacova et al., 2017). The yearly precipitation ranges from 1000–1500 mm in the mountains to 400–700 mm at the coast. About 45% of the annual precipitation is snow.

The Krycklan Catchment, located south of the Kalix River (Fig. 1), encompasses a natural mosaic of boreal landscapes consisting of forests, mires, streams, and lakes. The site provides the most advanced long-term field research facility in operation in a boreal biome (Laudon et al., 2013). The forest-dominated sampling station Västrabäcken (98.7% forest; 1.3% wetland; 0.12 km^2) is instrumented with continuous discharge measurement and stream water sampling. The main types of tree in the catchment of the first-order stream are Scots pine (64%) and Norway spruce (36%). The mean annual precipitation is 600 mm and about 50% falls as snow (Laudon et al., 2007). The first-order streams in the Krycklan catchment eventually drain into the Ume River. As in the Kalix River catchment, the soils are dominated by podzol profiles developed from locally derived till, except for the riparian zone, which has more organic soils (Lidman et al., 2017).

The composition of the catchments of Kalix and Ume River, respectively, is almost identical, both catchments consist mainly of forest, grassland and mires, with minor percentages of mountainous areas and lakes (SMHI, 2018). The main soils are moraine, peat, and thin soils. The similarity in geology, landscape type, and climate allows us to compare a first-order stream from the Krycklan catchment with the Kalix River.

3. METHODS

This study includes samples from three different sampling campaigns. The Kalix River was sampled at Kamlunge between April and October 2006 (23 samples). The

river at this station is about 100 m wide. Bulk water samples were collected about 4 m from land with acid-washed, metal-free sampling equipment (details, see Engström et al., 2010). Organic carbon concentrations are reported as total organic carbon (TOC). The organic carbon concentration was determined at Umeå Marine Science Centre, using a Shimadzu TOC-5000 high temperature catalytic oxidation instrument (Engström et al., 2010). In Kalix River and the Krycklan Catchment the TOC concentration is mainly determined by the DOC concentration (>93%) (Ingri et al., 2000; Laudon et al., 2004a,b; Neubauer et al., 2013). Iron concentrations were determined on the dissolved and the unfiltered samples, whereas Fe isotopes were only determined on the unfiltered samples. The first-order stream sampling was carried out between April and May 2011 in the Krycklan Catchment (Västrabäcken station). Samples were filtered in situ, using 0.22 μm nitrocellulose membrane filters (Millipore) mounted in polycarbonate filter holder. Both fractions (dissolved, <0.22 μm, and particulate, >0.22 μm) of the samples were analyzed for Fe concentrations and Fe isotopes. Although the spring flood episodes vary from year to year in terms of timing, runoff volume, and peak discharge, previous investigations of Fe in both, the Kalix River and the Krycklan Catchment, have demonstrated that the spring flood always follows the same patterns with respect to Fe (Andersson et al., 2006; Ingri et al., 2006; Björkvald et al., 2008).

The total Fe concentration in water can be defined in two ways. Water is filtered, and both the dissolved and the particulate fractions are analyzed separately, or measurements are done on acidified bulk (unfiltered) waters. Both methods are used in this study. Iron in bulk waters is referred to as Fe_{bulk}, particulate Fe as Fe_{part}, and dissolved Fe as Fe_{diss}. Dissolved Fe is defined as the fraction passing through a 0.22 μm filter, and particulate Fe as the fraction retained on the filter. It has been shown that the dissolved fraction is a mixture of truly dissolved Fe and Fe colloids (Ingri et al., 2000).

Soil water and groundwater were collected in November 2015 from soil lysimeters, which were installed at different depths in the riparian zone of Västrabäcken in 1995. The distance to the first-order stream is ca. 1 m measured perpendicularly and ca. 4 m measured along the flow direction of the groundwater. Since more than 20 years had passed from the installation of the lysimeters to the sampling of the water, no effects from the disturbance to the soil are believed to remain. The water was extracted by attaching acid-washed vacuum bottles to the tubes that are connected to each of the ceramic cups in the soil. This procedure will filter out any particles >1 μm (Grabs et al., 2012). The bottles were allowed to fill overnight, allowing sufficient volumes to be extracted, and were then collected the following day. Due to the relatively long sampling times that are required for soil water extraction the conservation of the Fe speciation could not be guaranteed so no attempts to distinguish particulate and dissolved fractions were made on these samples. The samples were brought to the Swedish University of Agricultural Sciences in Umeå, where they were stored cold and dark until they were sent directly for analysis the next day. The soils and the setup have been described in detail by Lidman et al. (2017). The TOC concentrations in the soil waters were taken from Lidman et al. (2017) and represent the annual average concentrations.

Dissolved, particulate, and bulk Fe concentrations were determined by Inductively Coupled Plasma Sector Field Mass Spectrometry (ICP-SFMS; Element 2, Thermo Fisher Scientific, Bremen, Germany), using external calibration combined with internal standardization. All samples and standards were matrices matched to a HNO_3 concentration of 0.3 molar. For more details, see Engström et al. (2010). Replicated measurements of each sample (n = 3) showed a precision of 2.5%. Limit of detection (3-times SD of blanks) was 0.0002 μM.

The Fe isotope ratios were measured on bulk water samples from 2006 and 2015 and on the dissolved and particulate phase from 2011 using Multi Collector Inductively Coupled Plasma Mass Spectrometry (MC-ICP-MS). Preconcentration was accomplished by evaporation of 150–500 ml of water using acid-washed Teflon beakers on a ceramic-top hotplate in a metal-free fume hood. After the first evaporation, solid residue was dissolved in 5 ml concentrated 15.6 M HNO_3, evaporated, 2 ml concentrated 12.1 M HCl was added to convert Fe into chloride form, evaporated. The residue was re-dissolved in 8 M HCl. No residues were observed after the digestion process. The filters were treated with a 1000:1 mixture of HNO_3/HF overnight followed by closed-vessel microwave-assisted digestion. Prior to analysis, the digests were further diluted in 10% HNO_3.

Iron was separated from matrix elements by ion exchange (for further details see Rodushkin and Ruth, 1997; Ingri et al., 2006). Mass balance estimations of each sample before and after the anion-exchange separation demonstrated a recovery rate of >95% for Fe. The ion exchange fraction containing Fe was evaporated to dryness and 50 μL of concentrated 15.6 M HNO_3 was pipetted directly to residue, what was followed by the addition of 5 ml MQ-water. For samples with relatively high Fe content, concentration in measurement solutions was adjusted to 2 mg L^{-1} by dilution with 1% HNO_3. Evaporated separates of water samples with low Fe concentrations were diluted to approximately 40–50 μg L^{-1} and measured using high-efficiency desolvation nebulizer (Aridus) in a separate analytical sequence. Isotope ratio measurements were performed by MC-ICP-MS (NEPTUNE and NEPTUNE PLUS). Instrumental mass-bias was corrected using a combination of internal standardization (Ni added at 5 mg L^{-1} to all measurement solutions) and bracketing isotope standards matching sample solutions in Fe concentration and acid strength. Delta values were calculated against the standard IRMM-14 CRM (Eq. (1)). Furthermore, in-house quality control samples (prepared by sequential dilutions of SPECTROSCAN 10,000 mg L^{-1} Fe element standard for atomic spectroscopy from TEKNOLAB, Drøbak, Norway) were analyzed at the beginning and the end of each analytical session, to ensure internal consistency of analytical results. The Fe isotope ratios in this material have been measured on a regular basis at ALS Scandinavia AB since 2003 (mean $\delta^{56}Fe$ of $-0.236 \pm 0.031‰$ (n > 120, one

sigma). This standard is a suitable reproducibility control for Fe isotope ratio measurements in the low fractionated samples (Malinovsky et al., 2003; Baxter et al., 2006). Each sample was measured twice with the sample-standard bracketing method. All Fe isotope data are reported in Tables 1–3 including 2σ (n = 4).

$$\delta^{56}Fe(‰) = \left[\frac{(^{56}Fe/^{54}Fe)_{sample}}{(^{56}Fe/^{54}Fe)_{IRMM-014}} - 1\right] * 10^3 \quad (1)$$

Lateral Fe fluxes in the soil profile were estimated based on the hydrological model for the investigated transect presented by Laudon et al. (2004a,b) and the Fe concentrations in soil water and groundwater from the same transect published by Lidman et al. (2017). Laudon et al. (2004a,b) demonstrated a strong relationship between groundwater levels in the investigated soil profile and runoff in the nearby first-order stream (Västrabäcken). Based on this link, stable water isotopes and the reported transmissivity feedback mechanism it was possible to estimate how much water is transported to the first-order stream in different depth intervals in the soil over time, and it was found that much of the groundwater transport occurred in a relatively narrow depth interval close to the groundwater surface (Laudon et al., 2004a,b; Bishop et al., 2011). In order to estimate where the Fe is transported to stream the water fluxes in each layer were multiplied by the average observed or interpolated (for depth intervals with no lysimeter) Fe concentration in each depth interval. This resulted in a depth distribution of Fe fluxes, indicating at what depths most of the Fe is transported to stream over time.

4. RESULTS

Bulk Fe concentrations in the Kalix River had a peak value at about 22 μM during spring flood in May 2006. The lowest values, about 4 μM, were seen in September (Table 1 and Fig. 2). Previous measurements have shown that about 40% of the yearly Fe transport from the Kalix River catchment occurs during spring flood in May (Pontér et al., 1990). In the first-order stream the total Fe concentration reached almost as high as in the Kalix River, approximately 20 μM, in connection with the spring flood (Table 2). Unlike the Kalix River, however, the transport in the first-order stream was strongly dominated by dissolved Fe (>90%). Previous studies at the first-order stream showed that the difference between concentrations in the dissolved phase and the total concertation are negligible (e.g. Laudon et al., 2004a,b; Neubauer et al., 2013). The highest Fe concentrations were observed in the soil water of the riparian zone of Västrabäcken, where concentrations up to 106 μM were observed. These high Fe concentrations in the riparian zone were consistent with previous measurements, and are believed to be related, to the high concentration of organic matter in this soil profile (Lidman et al., 2017).

All Kalix River bulk samples showed positive δ^{56}Fe values (Fig. 2). The Fe isotope composition of the bulk samples was fluctuating, but there was a systematic decrease during early spring flood, from about 0.5‰ (early-April) down to about 0.1‰ (mid-May discharge peak) (Fig. 2). The values during this period, showed a linear negative correlation between the Fe isotope composition of the bulk River water and the TOC/Fe_{bulk} ratio (Fig. 3). In the

Table 1
Kamlunge sampling in 2006. Iron concentrations, Fe isotope compositions, and TOC values.

Station	Date 2006	Fe_{diss} (μM)	Fe_{bulk} (μM)	$\delta^{56}Fe_{bulk}$ (‰)	2 σ (‰)	TOC (μM)
Kalix River	4-Apr	5.7	18.4	0.523	0.082	250
Kalix River	9-Apr	5.2	18.0	0.537	0.040	200
Kalix River	17-Apr	5.4	17.7	0.438	0.062	258
Kalix River	24-Apr	5.8	17.2	0.408	0.028	208
Kalix River	1-May	5.0	16.9	0.317	0.020	325
Kalix River	4-May	6.0	19.6	0.243	0.002	566
Kalix River	7-May	9.7	21.3	0.099	0.022	550
Kalix River	10-May	7.8	20.3	0.119	0.026	966
Kalix River	14-May	7.6	16.3	0.187	0.064	1516
Kalix River	18-May	5.6	13.0	0.191	0.078	908
Kalix River	22-May	3.6	12.3	0.241	0.150	458
Kalix River	25-May	4.0	11.1	0.002	0.034	416
Kalix River	28-May	2.5	10.6	0.076	0.084	408
Kalix River	4-Jun	2.5	7.9	0.211	0.012	400
Kalix River	10-Jun	2.3	7.0	0.216	0.084	383
Kalix River	19-Jun	3.3	6.6	0.261	0.036	300
Kalix River	27-Jun	2.8	5.5	0.349	0.030	266
Kalix River	7-Jul	2.4	4.9	0.159	0.054	233
Kalix River	24-Jul	1.9	4.6	0.224	0.064	208
Kalix River	9-Aug	0.3	4.2	0.047	0.012	175
Kalix River	21-Aug	1.3	4.0	−0.017	0.108	183
Kalix River	21-Sep	2.0	3.9	0.212	0.030	166
Kalix River	8-Oct	2.6	5.6	0.270	0.014	166

Table 2
Water samples from Västrabäcken, Krycklan (samples from 2011). Iron concentrations of the dissolved and particulate fraction, their Fe isotope compositions, and the TOC concentrations. The Fe_{bulk} concentrations are calculated by the Fe_{diss} and Fe_{part} concentrations.

Date 2011	Fe_{diss} (μM)	Fe_{part} (μM)	Fe_{diss}/Fe_{part}	Fe_{bulk} (μM)	$\delta^{56}Fe_{diss}$ (‰)	2 σ (‰)	$\delta^{56}Fe_{part}$ (‰)	2 σ (‰)	TOC (μM)
4-Apr	6.2	0.6	10	6.8	−0.449	0.094	−0.912	0.062	973
11-Apr	18.6	0.5	37	19.1	−0.461	0.170	−0.941	0.016	1790
14-Apr	19.9	0.2	100	20.1	−0.125	0.014	−0.695	0.090	2347
18-Apr	13.8	0.3	46	14.1	−0.079	0.096	−0.600	0.010	2443
21-Apr	13.8	0.2	69	14.0	−0.087	0.090	−0.576	0.048	2093
25-Apr	11.1	0.9	12	12.0	−0.116	0.074	−0.201	0.126	1929
2-May	12.1	0.3	40	12.4	−0.549	0.052	−0.970	0.130	1324
9-May	11.1	0.1	111	11.2	−0.395	0.012			1201

Table 3
Iron concentrations and Fe isotope compositions and the TOC concentrations of the soil profile in Västrabäcken, Krycklan (samples from 2015).

Sample	Depth cm	Fe_{bulk} (μM)	$\delta^{56}Fe_{bulk}$ ‰	2 σ ‰	TOC (μM)
S4-25	25	101.0	0.204	0.052	6007
S4-35	35	64.4	0.905	0.066	4557
S4-45	45	96.5	−0.095	0.058	3825
S4-55	55	106.0	−0.204	0.048	3022
S4-65	65	96.1	0.154	0.054	3347

first-order stream, dominated by forest, both dissolved and particulate Fe showed negative $\delta^{56}Fe$ values (<0‰), throughout the spring flood (Fig. 4). The particulate Fe fraction of the first-order stream was more negative (by approximately 0.5‰ points), compared to the dissolved fraction. Mass balance calculations showed that the Fe isotope composition of the bulk sample would be almost identical to the Fe isotope composition of the dissolved fraction (Fig. 4). The soil waters showed a transient change of the $\delta^{56}Fe$ value across the groundwater table from 0.9‰ to −0.1% (Table 3 and Fig. 5). Soil water samples below the groundwater table showed negative $\delta^{56}Fe$ values (−0.2‰). Fig. 6 compiles all Fe isotope data from this study in context with Fe isotope data from similar environments.

The transport of Fe from the riparian soil profile to the headwater stream was estimated to occur primarily in a relatively narrow depth interval (ca. 30–60 cm) close to where the groundwater level usually is found (Fig. 7). Since the vertical variation in Fe concentration in the soil water was comparatively low, the transport was largely controlled by the groundwater advection, which has been demonstrated to take place predominately at these depths, e.g. using ^{18}O as a tracer (Laudon et al., 2004a,b; Peralta-Tapia et al., 2015; Lidman et al., 2017). The active soil layers represent the so-called dominating source layer (DSL), as discussed by Ledesma et al. (2016).

5. DISCUSSION

Iron concentration data from the first-order stream mirrors the significant processes influencing Fe transport during annual spring discharge. Striking features of the first-

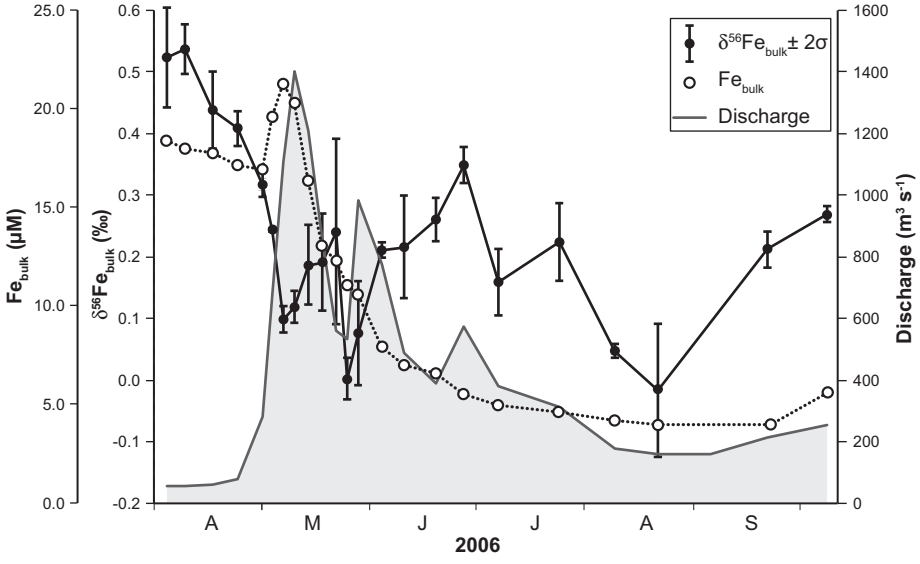

Fig. 2. Bulk (unfiltered) Fe concentrations and $\delta^{56}Fe_{bulk}$ in the Kalix River between April and September 2006. Note the systematic decrease of the $\delta^{56}Fe_{bulk}$ signal (becoming lighter) from winter base flow (April) to maximum spring discharge (May). The error bars represent ±1σ.

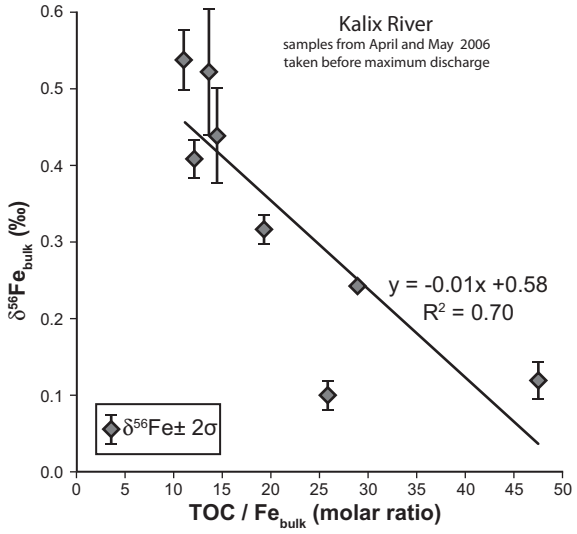

Fig. 3. Iron isotope composition versus the TOC/Fe_{bulk} molar ratio in the Kalix River, going from base flow in April to maximum spring flood in May (first 8 samples from Fig. 2, just before the Fe concentration starts to decline, sample 9).

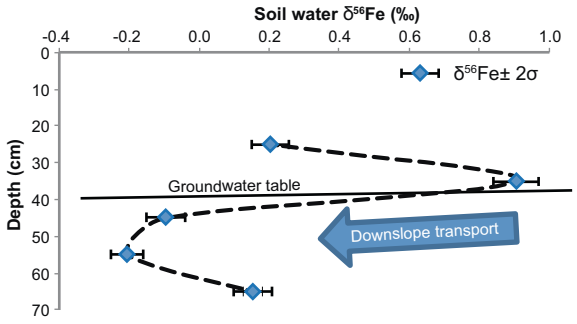

Fig. 5. Iron isotope concentration of a soil profile in Västrabäcken, Krycklan. The $\delta^{56}Fe$ changes from a heavy signal to a light signal at the groundwater table.

order stream are that both particulate and dissolved Fe has $\delta^{56}Fe$ values below 0.00‰ (Fig. 4) in contrast to the bulk river water samples showing only $\delta^{56}Fe$ values above 0.00‰ (Fig. 2). Furthermore, particulate $\delta^{56}Fe$ values are substantially lower (0.5‰ points) than that of dissolved Fe and there is a transient increase and a transient decrease (back to initial values at the low discharge period) in the Fe isotope composition (Fig. 4).

5.1. Origin of negative $\delta^{56}Fe$ values in the first-order stream

The oxidation of Fe(II) leads to the precipitation of Fe(III)-oxyhydroxides (e.g. Bullen et al., 2001; Johnson et al., 2002, 2004; Welch et al., 2003), which tend to be enriched in the heavy ^{57}Fe isotope. Furthermore, Teutsch et al. (2005) showed that adsorption of Fe(II) onto freshly precipitated Fe(III)oxyhydroxides leads to more negative Fe isotope compositions of the remaining soil water. Iron(II) is mobilized at low pH and low temperature in the upper organic-rich soil profile (O-horizon; Pokrovsky et al., 2006) during weathering and breakdown of organic litter. Several studies have shown that dissolved Fe(II) is partly oxidized and precipitates during transport in the unsaturated soil zone in podzols, causing migrating soil water Fe to be enriched in the light ^{56}Fe isotope (e.g. Beard et al., 1999, 2003; Brantley et al., 2004; Fantle and DePaolo, 2004; Wiederhold et al., 2006, 2007a,b; Thompson et al., 2007; dos Santos Pinheiro et al., 2014; Fekiacova et al., 2017). Furthermore, various studies have shown that anoxic groundwater is high in dissolved Fe(II) (Charette and Sholkovitz, 2002; Testa et al., 2002; Windom et al., 2006) and that its Fe isotope composition is negative relative to IRMM-014 (Teutsch et al., 2005). This is illustrated by the negative $\delta^{56}Fe$ values in the first-

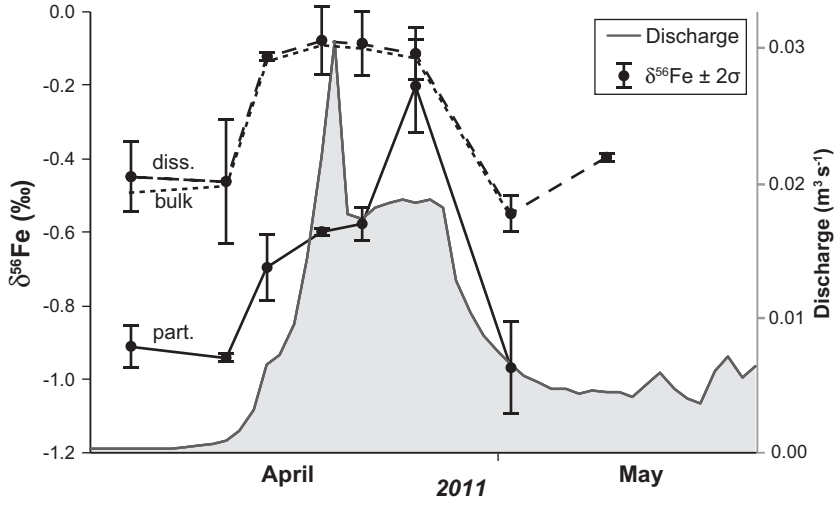

Fig. 4. Temporal variations in the Fe isotope composition in the dissolved (<0.22 μm) and particulate (>0.22 μm) fractions in a forested first-order stream (Västrabäcken, Krycklan, 2011) during spring flood. The $\delta^{56}Fe_{part}$ signature is about 0.5‰ lighter than the $\delta^{56}Fe_{diss}$ signature, but both fractions show negative Fe isotope signatures. The error bars represent ±2σ.

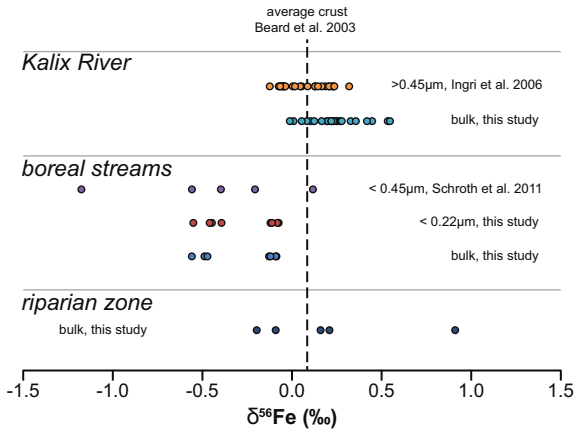

Fig. 6. Iron isotope composition of all samples from this study with reference data for average crust, the Kalix River dissolved phase, and dissolved data from another boreal stream (Schroth et al., 2011).

order stream before spring discharge when deeper and older groundwater dominates the discharge than during spring flood in the first-order streams. Furthermore, a negative δ^{56}Fe value ($-0.20‰ \pm 0.05‰$) was measured in the riparian soil pore water below the groundwater table (Fig. 5). Therefore, soil water might export negative Fe isotope compositions to groundwater (and successively into the first-order stream waters), leaving the soil enriched in the heavy ^{57}Fe isotope. This shows the direct connection between first-order streams and soil water. Ilina et al. (2013) showed that the dissolved Fe fraction in the small streams is a mixture of truly dissolved Fe and Fe colloids. They measured increasing Fe isotope values with decreasing colloid size, i.e. small sized organic-rich colloids were positive, while large sized mineral-rich colloids, were negative compared to IRMM-014. This suggests that the dominating colloids in the dissolved phase may have changed throughout the sampling. Larger colloids, with a negative Fe isotope composition, dominate the first-order stream, whereas the more positive values during spring discharge are most likely due to smaller organic-rich colloids. This would be consistent with the higher concentration of DOC in connection with the spring flood as a result of the activation of shallower, more organic soil layers (Laudon et al., 2011).

5.2. The transient change of the Fe isotope composition during spring flood in the first-order stream

Riparian zones in first-order streams are important sources of DOC (and related Fe), and often just a narrow dominant source layer (DSL) within the riparian profile is responsible for most of the export (Seibert et al., 2009; Grabs et al., 2012; Ledesma et al., 2015). Vertical concentration gradients in the riparian zone can therefore lead to transient changes in water chemistry and isotope compositions during high water discharge (Bishop et al., 2008; Seibert et al., 2009; Lidman et al., 2011). At the interface between anoxic-oxic soil water, which should be located near the groundwater table between 35 and 45 cm depth in the analyzed profile, the Fe isotope composition of the soil water changed from $-0.10‰ \pm 0.06‰$ below the groundwater table to $0.91‰ \pm 0.07‰$ above. This sharp gradient suggests that Fe is involved in redox reactions near the groundwater table in the riparian zone. Such shifts in the redox conditions close to the groundwater level are consistent with previous observations of selenium at the same site (Lidman et al., 2011). As a result of the sharp gradient, even a small change in the groundwater level will instantly change the isotope signal of the Fe exported to the first-order stream. The DSL concept can be defined as the narrow depth range within the riparian zone having the highest

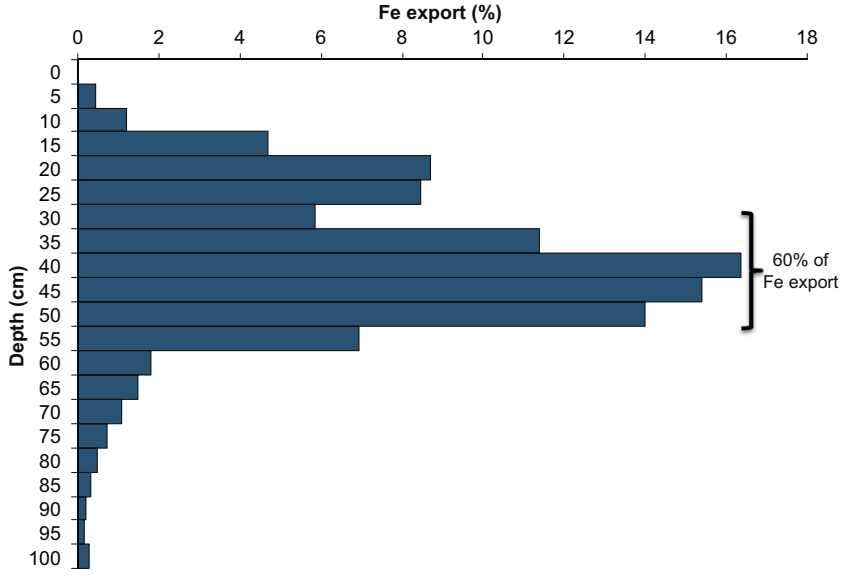

Fig. 7. Calculated Fe export within the riparian zone soil profile. Approximately 60% of the Fe transport is concentrated to a 20 cm layer between 35 and 55 cm depth at the time of sampling.

contribution to solute and water fluxes to the first-order stream (Ledesma et al., 2016). This idea is based on the exponential decrease in hydraulic conductivity with depth in the riparian zone implying that lateral flow paths converge to a relatively narrow layer, as suggested by Schiff et al. (1998), and this has been confirmed by ^{18}O studies at this site (Laudon et al., 2004a,b; Peralta-Tapia et al., 2015). The export of Fe was calculated for different depths in the soil profile, illustrating the transient changes in Fe transport in the soil water profile. Approximately 60% of the annual Fe transport was estimated to be concentrated to a 20 cm layer between 35 and 55 cm depth, which is close to where the groundwater level mostly is located (Fig. 7). The high contribution to the Fe transport of these soil layers was not unexpected given that so much of the groundwater transport to the stream occurs at these depths (Laudon et al., 2004a,b; Peralta-Tapia et al., 2015). Since the vertical variation in Fe concentration in the soil profile is relatively modest, the Fe transport will be almost exclusively controlled by the groundwater transport (Table 3; Lidman et al., 2017). As a consequence, processes affecting the Fe isotope composition in these soil layers can be expected to have a strong impact on the Fe isotope composition observed in the first-order stream.

The DSL concept, demonstrated in Fig. 7, can explain transient changes in the Fe isotope composition in the first-order stream (Ledesma et al., 2016). However, the Fe isotope compositions of the riparian soil water represent one single sampling occasion, so it remains unknown to what extent the Fe isotope signal at different depths varies throughout the year. It might be expected from the sharp gradients in the Fe isotope composition that there also are pronounced temporal variation, especially in soil horizons that alternate between the saturated and the unsaturated zone. Seasonal variations might therefore explain why none of the lysimeters in the riparian zone had a $\delta^{56}Fe$ signal that was quite as low as the particulate phase in the first-order stream during winter baseflow (ca. −0.45‰), but the overall pattern with higher $\delta^{56}Fe$ values in connection with the spring flood (up to −0.08‰) was consistent with a rising groundwater level and the resulting activation of shallower soil horizons with higher $\delta^{56}Fe$ values. Previous investigations of this soil profile have also shown that the Fe concentration of the soil water tends to be somewhat higher than in the adjacent first-order stream (Västrabäcken) (Lidman et al., 2017). This pattern of higher concentrations in the riparian zone was typical for organophilic elements, and the enrichment in the riparian soil water could be directly linked to the affinity for organic matter. Lidman et al. (2017) proposed that a likely explanation to the higher concentrations in the riparian soil water compared to the stream was that the riparian zone at this site had somewhat higher content of organic matter than the riparian zone along this stream in general. Nevertheless, the riparian soil water was found to be much more similar to the stream water than soil water from uphill podzols or deeper groundwater, so the stream water chemistry still displayed a clear signal from the riparian zone. Therefore, there are good reasons to believe that the changes in Fe isotope composition that were observed in this soil water profile reflect processes that Fe is involved in, as it is being transported towards the stream. Further research will have to clarify to what extent these patterns vary spatially (e.g. along this particular stream and at other sites) and temporally (e.g. in connection with rising and falling groundwater tables during the spring flood), but the presented data suggest that Fe is highly active in the riparian zone and that there may be considerable spatiotemporal variation in the Fe isotope composition. Fekiacova et al. (2013) classified soil profiles by the difference between the highest and the lowest $\delta^{56}Fe$ value within one profile ($\Delta^{56}Fe$). Podzol profiles showed a significant fractionation along the vertical profile and a $\Delta^{56}Fe > 0.15‰$. The soil water profile in the riparian zone had a $\Delta^{56}Fe$ of 1.1‰, suggesting that acidic pH conditions lead to the dissolution of Fe(III) and the subsequent translocation of released light Fe by organic matter (Fekiacova et al., 2013). The light Fe could precipitate in deeper layers of the soil profile, leading to a significant isotope fractionation.

As the spring flood begins in the forest landscape, the $\delta^{56}Fe$ signal increases in the first-order stream, while it decreases in the Kalix River until they both reach an interval near 0 (ca. −0.1 to 0.2‰; Figs. 2 and 4). Because the snowmelt in the forests precedes the snowmelt in the mountains, the river should be dominated by water from the forest landscape at this point, and therefore small first-order streams like Västrabäcken should be a major source for Fe. During this period the Fe isotope composition in both, first-order stream water and river water, coincide with the observed signature in riparian groundwater (Fig. 5).

Although both the Kalix River and the first-order stream carry similar Fe concentrations, they display contrasting patterns in the $\delta^{56}Fe$ signal. The measurements in Västrabäcken suggest that the first-order stream value is negative (ca. −0.5‰) during baseflow conditions, while the Kalix River at this time displays a distinct heavy signal (ca. +0.5‰). This suggests that forest soils are not the primary Fe source in larger rivers during base flow conditions. Instead deeper groundwater and water from the mountain areas are likely to dominate the Kalix River during periods of low flow (Engström et al., 2010). During the snowmelt in the forest landscape, however, the Fe $\delta^{56}Fe$ signal in the Kalix River coincides with that of Västrabäcken, suggesting that the type of headwater streams that it represents are likely to be the major source of Fe during this period. Although it is a small stream compared to the Kalix River, this type of headwater streams is very common and stand for a substantial part of the runoff generation in the boreal forest landscape (Bishop et al., 2008).

5.3. Fe isotope compositions in the dissolved and particulate phase

Both dissolved and particulate Fe in the first-order stream showed Fe isotope values below 0.00‰, which should be expected if there is a substantial precipitation of Fe(III) in the B-horizons of upslope podzol soils (Fig. 4). Schuth et al. (2015) assumed that in oxidized soil solution Fe is present as Fe(II)/(III) in colloidal form possibly complexed by organic ligands, whereas at reducing

conditions Fe occurs as Fe^{2+} and as colloidal Fe(II)/(III). They concluded that reducing conditions in the topsoil with accumulated organic matter (O-horizon), as flooding or ponding will mobilize Fe and partially translocate it. The residual Fe pool in the soil will be depleted in ^{54}Fe relative to ^{56}Fe, whereas the soil solution will be enriched in ^{54}Fe. The soil solution might imprint the underlying illuviated layer (B-horizon) and, if oversaturated, migrate into local streams and rivers. Furthermore, Neubauer et al. (2013) showed that the Fe speciation changes along the flow path going from acidic water (pH 3.9) with high TOC concentration, as in Västrabäcken, to less acidic higher order streams (pH 6.4) with lower TOC concentration.

In the first-order stream, the dissolved fraction had a heavier isotopic signature compared to the particulate fraction, similar to the two groups of Fe colloids and particles observed in other studies (Fig. 8). Ingri et al. (2000) showed with ultrafiltration measurements that colloidal particles dominate element transport in the dissolved fraction during high discharge. We use the conceptual model discussed by Raiswell and Canfield (2012) to illustrate the major Fe aggregates in forest stream water (Fig. 8). These Fe aggregates consist of Fe particles and colloids that resemble to Fe(III)oxyhydroxides and organic-rich Fe aggregates (Raiswell and Canfield, 2012). We propose that the co-precipitated Fe(II)(III)-OC aggregate has a lighter isotopic signature compared to Fe(III)-oxyhydroxide, due to admixed isotopically light Fe(II) in the Fe(II)(III)-OC aggregate. This can be used to explain the isotopic variations observed at different scales. Natural Fe colloids are progressively enriched in heavy ^{57}Fe isotopes with decreasing size (Ilina et al., 2013). The dissolved fraction in the first-order stream is most likely composed of small Fe oxyhydroxide colloids, which are oxidized to a higher degree (less organic carbon) than the particles (Neubauer et al., 2013). As previously demonstrated by Sundman et al. (2014) in this soil profile, organically bound Fe(II) can remain unreactive even under oxidizing conditions. The enrichment of the heavy ^{57}Fe in the colloidal fraction could also be related to the negative Fe isotope composition of the dissolved phase in the first-order stream water during base flow, since this water tends to derive from deeper soil layers with more reducing conditions (Laudon et al., 2004a,b; Peralta-Tapia et al., 2015).

5.4. Mixing of two Fe components in the river

The systematic change in the bulk Fe isotope composition during spring flood in the Kalix River indicates that the Fe isotope value becomes more positive with decreasing TOC/Fe_{bulk} ratio and more negative with increasing TOC/Fe_{bulk} (Fig. 3). This is in agreement with Ilina et al. (2013) and Mulholland et al. (2015). This suggests that a low TOC/Fe_{bulk} ratio indicates Fe-oxyhydroxides as the dominant phase, while a high ratio indicates the dominance of co-precipitated Fe-OC. The linear negative correlation between the Fe isotope composition of the unfiltered river waters and the TOC/Fe_{bulk} ratio (Fig. 3) is consistent with mixing of two major types of Fe aggregates in the river, with different Fe isotope values during spring flood. The colloidal phase in these aggregates varies throughout the year. Andersson et al. (2006) showed that in the colloidal phase OC is dominating Fe transport in the Kalix River during spring flood in May. During base flow in winter Fe-rich colloids with little OC dominate the system.

Sundman et al. (2014) showed that the first-order stream analyzed in this study contains two major types of Fe aggregates, Fe(II)(III)–OC aggregates and Fe(III)oxyhydroxides. The presence of Fe(II) in Fe-OC aggregates has been shown in several studies even when the waters are well oxidized (e.g., Gaffney et al., 2008; Sundman et al., 2014; von der Heyden et al., 2014). The ratio OC/Fe seems to

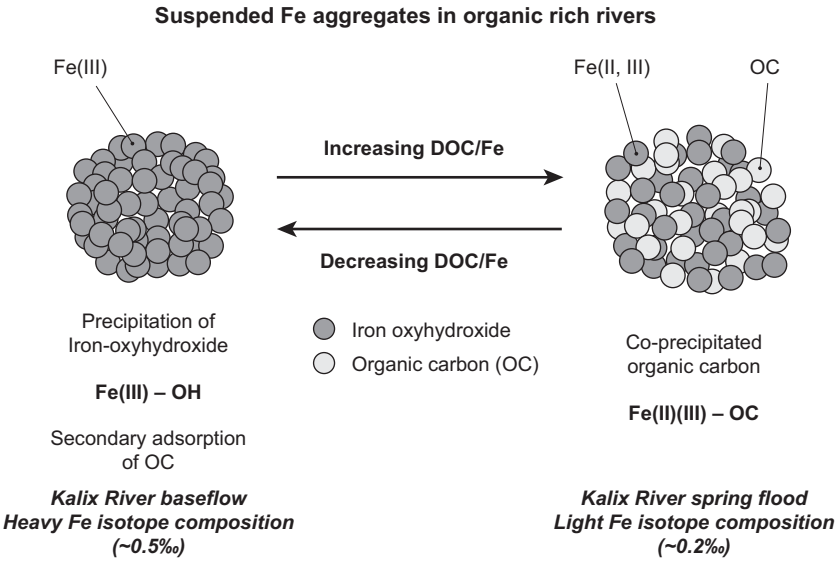

Fig. 8. Two types of Fe aggregates formed in boreal freshwater, based on a conceptual model discussed by Raiswell and Canfield (2012). We suggest that Fe(III)oxyhydroxides typically show a heavier Fe isotope composition than the lighter Fe-OC aggregates, with an admixed oxidation state of Fe(II)/(III).

be one of the major factors controlling the Fe isotope composition of colloids (Ilina et al., 2013). Ilina et al. (2013) suggested that large organic-rich colloids and particles are formed at the interface between anoxic soil and shallow groundwater and organic-rich oxidized surface water. Changes in the groundwater table are therefore likely to have a substantial impact on the Fe isotope composition in soil water and, successively, the first-order streams and the large-scale Fe transport. The strong fractionation of Fe isotopes close to the groundwater surface in the riparian zone is consistent with this hypothesis.

6. CONCLUSIONS

The combination of Fe isotope data from a riparian soil profile, a first-order stream, and a river, close to its outlet, allowed us to study the transformation of Fe isotopes along a boreal catchment. The observed Fe isotope variations could be explained by (i) different Fe aggregates in first-order stream water, where the co-precipitated Fe(II)(III)-OC aggregate has a lighter isotopic signature compared to Fe(III)oxyhydroxide, due to admixed isotopically light Fe(II) in the Fe(II)(III)-OC aggregate and (ii) different Fe sources for the river throughout the year. The different Fe isotope values in the Kalix River and the first-order stream during base flow conditions suggest that the forest soils cannot be the primary Fe source for the river, whereas the Fe isotope values during the spring flood suggest the riparian soil as source for Fe in the first-order stream and the river. This is consistent with the hydrological understanding of these systems. Sharp vertical gradients in the Fe isotope composition of riparian soil water, especially close to the groundwater table where much of the Fe transport to the stream networks occurs, suggested that Fe is highly active in these soils. More measurements on the spatiotemporal variation of Fe isotopes in riparian soils are needed to fully understand the transport of Fe through the riparian zone.

ACKNOWLEDGEMENTS

We wish to thank the Swedish Research Council and the Marie Curie network, MetTrans (Project number 290336), for their support of this study. We also want to thank Hjalmar Laudon for his help during sampling in Krycklan catchment. We thank Bio4Energy, a Strategic Research Environment appointed by the Swedish government, for supporting this work. Furthermore, we would like to thank the editors and reviewers for their time and work they spent to help to improve this manuscript.

APPENDIX A. SUPPLEMENTARY MATERIAL

Supplementary data associated with this article can be found, in the online version, at https://doi.org/10.1016/j.gca.2018.07.030.

REFERENCES

Allard T., Menguy N., Salomon J., Calligaro T., Weber T., Calas G. and Benedetti M. F. (2004) Revealing forms of iron in riverborne material from major tropical rivers of the Amazon Basin (Brazil). *Geochim. Cosmochim. Acta* **68**, 3079–3094.

Anbar A. D., Jarzecki A. A. and Spiro T. G. (2005) Theoretical investigations of iron isotope fractionation between $Fe(H_2O)_6^{3+}$ and $Fe(H_2O)_6^{2+}$: implications for iron stable isotope geochemistry. *Geochim. Cosmochim. Acta* **69**, 825–837.

Anderson H. A., Berrow M. L., Farmer V. C., Hepburn A., Russel J. D. and Walker A. D. (1982) A reassessment of podzol formation processes. *J. Soil Sci.* **33**, 125–136.

Andersson K., Dahlqvist R., Turner D., Stolpe B., Larsson T., Ingri J. and Andersson P. (2006) Colloidal rare earth elements in a boreal river: changing sources and distributions during the spring flood. *Geochim. Cosmochim. Acta* **70**, 3261–3274.

Baxter D. C., Rodushkin I., Engström E. and Malinovsky D. (2006) Revised exponential model for mass bias correction using an internal standard for isotope abundance ratio measurements by multi-collector inductively coupled plasma mass spectrometry. *J. Analyt. Atom. Spectrom.* **21**, 427–430.

Beard B. L., Johnson C. M., Cox L., Sun H., Nealson H. and Aguilar C. (1999) Iron isotope biosignatures. *Science* **285**, 1889–1892.

Beard B. L., Johnson C. M., von Damm K. L. and Poulson R. L. (2003) Iron isotope constraints on Fe cycling and mass balance in oxygenated Earth oceans. *Geology* **31**, 629–632.

Bergquist B. A. and Boyle E. A. (2006) Iron isotopes in the Amazon River system: weathering and transport signatures. *Earth Planet. Sci. Lett.* **248**, 54–68.

Bishop K., Buffam I., Erlandsson M., Fölster J., Laudon H., Seibert J. and Temnerud J. (2008) Aqua incognita: the unknown headwaters. *Hydrol. Process.* **22**, 1239–1242.

Bishop K., Seibert J., Nyberg L. and Rodhe A. (2011) Water storage in a till catchment. II: Implications of transmissivity feedback for flow paths and turnover times. *Hydrol. Process.* **25**, 3950–3959.

Björkvald L., Buffam I., Laudon H. and Mörth C.-M. (2008) Hydrogeochemistry of Fe and Mn in small boreal streams: the role of seasonality, landscape type and scale. *Geochim. Cosmochim. Acta* **72**, 2789–2804.

Brantley S. L., Liermann L. J., Guynn R. L., Anbar A., Icopini G. A. and Barling J. (2004) Fe isotopic fractionation during mineral dissolution with and without bacteria. *Geochim. Cosmochim. Acta* **68**, 3189–3204.

Bullen T. D., White A. F., Childs C. W., Vivit D. V. and Schulz M. S. (2001) Demonstration of significant abiotic iron isotope fractionation in nature. *Geology* **29**, 699–702.

Buurman P. and Jongmans A. G. (2005) Podzolisation and soil organic matter dynamics. *Geoderma* **125**, 71–83.

Charette M. A. and Sholkovitz E. R. (2002) Oxidative precipitation of groundwater-derived ferroous iron in the subterranean estuary of a coastal bay. *Geophys. Res. Lett.* **29, 10**, 85-1-85-4.

Cornu S., Montagne D. and Vasconcelos P. M. (2009) Dating constituent formation in soils to determine rates of soil processes: a review. *Geoderma* **153**, 293–303.

Dahlqvist R., Andersson K., Ingri J., Larsson T., Stolpe B. and Turner D. (2007) Temporal variations of colloidal carrier phases and associated trace elements in a boreal river. *Geochim. Cosmochim. Acta* **71**, 5339–5354.

dos Santos Pinheiro G. M., Poitrasson F., Sondag F., Cochonneau G. and Vieira L. C. (2014) Contrasting iron isotopic compositions in river suspended particulate matter: the Negro and the Amazon annual river cycles. *Earth Planet. Sci. Lett.* **394**, 168–178.

Emmanuel S., Erel Y., Matthews A. and Teutsch N. (2005) A preliminary mixing model for Fe isotopes in soils. *Chem. Geol.* **222**, 23–34.

Engström E., Rodushkin I., Ingri J., Baxter D. C., Ecke F., Österlund H. and Öhlander B. (2010) Temporal isotopic variations of dissolved silicon in a pristine boreal river. *Chem. Geol.* **271**, 142–152.

Escoube R., Rouxel O. J., Sholkovitz E. and Donard O. F. X. (2009) Iron isotope systematics in estuaries: the case of North River, Massachusetts (USA). *Geochim. Cosmochim. Acta* **73**, 4045–4059.

Escoube R., Rouxel O. J., Pokrovsky O. S., Schroth A., Max Holmes R. and Donard O. F. X. (2015) Iron isotope systematics in Arctic rivers. *CR Geosci.* **347**, 377–385.

Fantle M. S. and DePaolo D. J. (2004) Iron isotopic fractionation during continental weathering. *Earth Planet. Sci. Lett.* **228**, 547–562.

Fekiacova Z., Pichat S., Cornu S. and Balesdent J. (2013) Inferences from the vertical distribution of Fe isotopic compositions on pedogenetic processes in soils. *Geoderma* **209–210**, 110–118.

Fekiacova Z., Vermeire M. L., Bechon L., Cornelis J. T. and Cornu S. (2017) Can Fe isotope fractionations trace the pedogenetic mechanisms involved in podsolization? *Geoderma* **296**, 38–46.

Fromm E. (1965) Beskrivning till jordartskartan over norrbottens län, nedanför lappmarkdsgränsen. *SGU ser Ca* **41**, 1–151 (in Swedish with English summary).

Gaál G. and Gorbatschev R. (1987) An outline of the Precambrian evolution of the Baltic Shield. *Precambrian Res.* **35**, 15–52.

Gaffney J. W., White K. N. and Boult S. (2008) Oxidation state and size of Fe controlled by organic matter in natural waters. *Environ. Sci. Technol.* **42**, 3575–3581.

Grabs T., Bishop K., Laudon H., Lyon S. W. and Seibert J. (2012) Ripar- ian zone hydrology and soil water total organic carbon (TOC): implications for spatial variability and upscaling of lateral riparian TOC exports. *Biogeosciences* **9**, 3901–3916. https://doi.org/10.5194/bg-9-3901-2012.

Hamon R., Batley G. E. and Casey P. (2005) Environmental nanovectors: an emerging science area. *SETAC Globe* **6**(4), 21–22.

Huang L. M., Jia X.-X., Zhang G.-L., Thompson A., Huang F., Shao M.-A. and Chen L.-M. (2018) Variations and controls of iron oxides and isotope compositions during paddy soil evolution over a millennial time scale. *Chem. Geol.* **476**, 340–351.

Ilina S. M., Poitrasson F., Lapitskiy S. A., Alekhin Y. V., Viers J. and Pokrovsky O. S. (2013) Extreme iron isotope fractionation between colloids and particles of boreal and temperate organic-rich waters. *Geochim. Cosmochim. Acta* **101**, 96–111.

Ingri J. and Widerlund A. (1994) Uptake of alkali and alkaline-earth elements on suspended iron and manganese in the Kalix River, northern Sweden. *Geochim. Cosmochim. Acta* **58**, 5433–5442.

Ingri J., Widerlund A., Land M., Gustafsson Ö., Andersson P. and Öhlander B. (2000) Temporal variations in the fractionation of the rare earth elements in a boreal river; the role of colloidal particles. *Chem. Geol.* **166**, 23–45.

Ingri J., Widerlund A. and Land M. (2005) Geochemistry of major elements in a pristine boreal river system; Hydrological compartments and Flow paths. *Aquat. Geochem.* **11**, 57–88.

Ingri J., Malinovsky D., Rodushkin I., Baxter D. C., Widerlund A., Andersson P., Gustafsson Ö., Forsling W. and Öhlander B. (2006) Iron isotope fractionation in river colloidal matter. *Earth Planet. Sci. Lett.* **245**, 792–798.

Johnson C. M., Skulan J. L., Beard B. L., Sun H., Nealson K. H. and Braterman P. S. (2002) Isotopic fractionation between Fe (III) and Fe(II) in aqueous solutions. *Earth Planet. Sci. Lett.* **195**, 141–153.

Johnson C. M., Beard B. L., Roden E. E., Newman D. K. and Nealson K. H. (2004) Isotopic constraints on biogeochemical cycling of Fe. In *Geochemistry of Non-Traditional Stable Isotopes* (eds. C. M. Johnson, B. L. Beard and F. Albarède), pp. 359–408.

Laudon H., Köhler S. and Buffam I. (2004a) Seasonal TOC export from seven boreal catchments in northern Sweden. *Aquat. Sci.* **66**, 223–230.

Laudon H., Seibert J., Kohler S. and Bishop K. (2004b) Hydrological flow paths during snowmelt: congruence between hydrometric measurements and oxygen 18 in meltwater, soil water, and runoff. *Wat. Resour. Res.*, 40.

Laudon H., Sjöblom V., Buffam I., Seibert J. and Mörth M. (2007) The role of catchment scale and landscape characteristics for runoff generation of boreal streams. *J. Hydrol.* **344**, 198–209.

Laudon H., Berggren M., Ågren A., Buffam I., Bishop K., Grabs T., Jansson M. and Köhler S. (2011) Patterns and Dynamics of Dissolved Organic carbon (DOC) in Boreal Streams: The Role of Processes, Connectivity, and Scaling. *Ecosystems* **14**, 880–893.

Laudon H., Tabermann I., Ågren A., Futter M., Ottosson-Löfvenius M. and Bishop K. (2013) The Krycklan Catchment Study—a flagship infrastructure for hydrology, biogeochemistry, and climate research in the boreal landscape. *Wat. Resour. Res.* **49**, 7154–7158.

Ledesma J., Grabs T., Bishop K. H., Schiff S. L. and Köhler S. J. (2015) Potential for long-term transfer of dissolved organic carbon from riparian zones to streams in boreal catchments. *Glob. Change Biol.* **21**, 2963–2979.

Ledesma J., Futter M. N., Laudon H., Evans C. D. and Köhler S. J. (2016) Boreal forest riparian zones regulate stream sulfate and dissolved organic carbon. *Sci. Tot. Environ.* **560–561**, 110–122.

Lidman F., Mörth C.-M., Björkvald L. and Laudon H. (2011) Selenium dynamics in boreal streams: the role of wetlands and changing groundwater tables. *Environ. Sci. Technol.* **45**, 2677–2683.

Lidman F., Boily Å., Laudon H. and Köhler S. J. (2017) From soil water to surface water – how the riparian zone controls element transport from a boreal forest to a stream. *Biogeoscienes* **14**, 3001–3014.

Lundström U. S., van Breemen N. and Bain D. (2000) The podsolization process. A review. *Geoderma* **94**, 91–107.

Malinovsky D., Stenberg A., Rodushkin I., Andren H., Ingri J., Öhlander B. and Baxter D. C. (2003) Performance of high resolution MC-ICP-MS for Fe isotope ratio measurements in sedimentary geological materials. *J. Anal. At. Spectrom.* **18**, 687–695.

Mulholland D. S., Poitrasson F., Boaventura G. R., Allard T., Cruz Vieira L., Ventura Santos R., Mancini L. and Seyler P. (2015) Insights into iron sources and pathways in the Amazon River provided by isotopic and spectroscopic studies. *Geochim. Cosmochim. Acta* **150**, 142–159.

Neubauer E., Köhler S. J., von der Kammer F., Laudon H. and Hofmann T. (2013) Effect of pH and stream order on iron and arsenic speciation in boreal catchments. *Environ. Sci. Technol.* **47**, 7120–7128.

Patel-Sorrentino N., Lucas Y., Eyrolle F. and Melfi A. J. (2007) Fe, Al and Si species and organic matter leached off a ferrallitic and podzolic soil system from Central Amazonia. *Geoderma* **137**, 444–454.

Peralta-Tapia A., Sponseller R. A., Tetzlaff D., Soulsby C. and Laudon H. (2015) Connecting precipitation inputs and soil flow pathways to stream water in contrasting boreal catchments. *Hydrol. Proc.* **29**, 3546–3555.

Poitrasson F., Viers J., Martin F. and Braun J.-J. (2008) Limited iron isotope variations in recent lateritic soils from Nsimi, Cameroon: implications for the global Fe geochemical cycle. *Chem. Geol.* **253**, 54–63.

Polyakov V. B. and Mineev S. D. (2000) The use of Mössbauer spectroscopy in stable isotope geochemistry. *Geochim. Cosmochim. Acta* **64**, 849–865.

Pontér C., Ingri J., Burman J.-O. and Boström K. (1990) Temporal variations in dissolved and suspended iron and manganese in the Kalix River, northern Sweden. *Chem. Geol.* **81**, 121–131.

Pokrovsky O. S. and Schott J. (2002) Iron colloids/organic matter associated transport of major and trace elements in small boreal rivers and their estuaries (NW Russia). *Chem. Geol.* **190**, 141–179.

Pokrovsky O. S., Schott J. and Dupré B. (2006) Trace element fractionation and transport in boreal rivers and soil porewaters of permafrost-dominated basaltic terrain in Central Siberia. *Geochim. Cosmochim. Acta* **70**, 3239–3260.

Raiswell R. and Canfield D. E. (2012) The iron biogeochemical cycle past and present. *Geochem. Perspect.* **1**, 1–220.

Rodushkin I. and Ruth T. (1997) Determination of trace metals in estuarine and sea-water reference materials by high resolution inductively coupled plasma mass spectrometry. *J. Analyt. Atom. Spectrom.* **12**, 1181–1185.

Sauer D., Sponagel H., Sommer M., Giani L., Jahn R. and Stahr K. (2007) Podzol: soil of the year 2007. A review on its genesis, occurrence, and functions. *J. Plant Nutr. Soil Sci.* **170**, 581–597.

Sauer D., Schülli-Maurer I., Sperstad R., Sørensen R. and Stahr K. (2008) Podzol development with time in sandy beach deposits in southern Norway. *J. Plant Nutr. Soil Sci.* **171**, 483–497.

Schiff S., Aravena R., Mewhinney E., Elgood R., Warner B., Dillon P. and Trumbore S. (1998) Precambrian shield wetlands: hydrologic control of the sources and export of dissolved organic matter. *Climatic Change* **40**, 167–188.

Schroth A. W., Crusius J., Chever F., Bostick B. C. and Rouxel O. J. (2011) Glacial influence on the geochemistry or riverine iron fluxes to the Gulf of Alaska and effects of deglaciation. *Geophys. Res. Lett.* **38**, L16605.

Schuth S., Hurrass J., Muenker C. and Mansfeldt T. (2015) Redox-dependent fractionation of iron isotopes in suspensions of a groundwater-influenced soil. *Chem. Geol.* **392**, 74–86.

Seibert J., Grabs T., Köhler S., Laudon H., Winterdahl M. and Bishop K. (2009) Linking soil- and stream–water chemistry based on a riparian flow-concentration integration model. *Hydrol. Earth Syst. Sci.* **13**, 2287–2297.

Swedish meterological and hydrological institute, vattenwebb.smhi.se.

Sundman A., Karlsson T., Laudon H. and Persson P. (2014) XAS study of iron speciation in soils and waters from a boreal catchment. *Chem. Geol.* **364**, 93–102.

Testa J. M., Charette M. A., Sholkovitz E. R., Allen M. C., Rago A. and Herbold C. W. (2002) Dissolved iron cycling in the subterranean estuary of a coastal bay: Waquoit Bay, Massachusetts. *Biol. Bull.* **203**, 255–256.

Teutsch N., von Gunten U., Porcelli D., Cirpka O. A. and Halliday A. N. (2005) Adsorption as a cause for iron isotope fractionation in reduced groundwater. *Geochim. Cosmochim. Acta* **69**, 4175–4185.

Thompson A., Ruiz J., Chadwick O. A., Titus M. and Chorover J. (2007) Rayleigh fractionation of iron isotopes during pedogenesis along a climate sequence of Hawaiian basalt. *Chem. Geol.* **238**, 72–83.

Von der Heyden B. P., Hauser E. J., Mishra B., Martinez G. A., Bowie A. R., Tyliszczak T., Mtshali T. N., Roychoudhury A. N. and Myneni S. C. (2014) Ubiquitous presence of Fe (II) in aquatic colloids and its association with organic carbon. *Environ. Sci. Technol. Lett.* **1**, 387–392.

Welch S. A., Beard B. L., Johnson C. M. and Braterman P. S. (2003) Kinetic and equilibrium Fe isotope fractionation between aqueous Fe (II) and Fe(III). *Geochim. Cosmochim. Acta* **67**, 4231–4250.

Wiederhold J. G., Kraemer S. M., Teutsch N., Borer P. M., Halliday A. N. and Kretzschmar R. (2006) Iron isotope fractionation during proton-promoted, ligand-controlled, and reductive dissolution of goethite. *Environ. Sci. Technol.* **40**, 3787–3793.

Wiederhold J. G., Teutsch N., Kraemer S. M., Halliday A. N. and Kretzschmar R. (2007a) Iron isotope fractionation in oxic soils by mineral weathering and podsolization. *Geochim. Cosmochim. Acta* **71**, 5821–5833.

Wiederhold J. G., Teutsch N., Kraemer S. M., Halliday A. N. and Kretzschmar R. (2007b) Iron isotope fractionation during pedogenesis in redoximorphic soils. *Soil Sci. Soc. Am. J.* **71**(6), 1840–1850.

Windom H. L., Moore W. S., Niencheski L. F. H. and Jahnke R. A. (2006) Submarine groundwater discharge: a large, previously unrecognized source of dissolved iron to the South Atlantic Ocean. *Mar. Chem.* **102**, 252–266.

Associate editor: Martin Novak